Journal of Computational Physics 231 (2012) 7881–7892

Contents lists available at SciVerse ScienceDirect

Journal of Computational Physics

journal homepage: www.elsevier.com/locate/jcp

Boundary treatment effects on molecular dynamics simulations of interface thermal resistance

Murat Barisik, Ali Beskok *

Old Dominion University, Institute of Micro and Nanotechnology, Mechanical & Aerospace Engineering Department, Norfolk, VA 23529-0247, USA

ARTICLE INFO

Article history:
Received 22 December 2011
Received in revised form 17 July 2012
Accepted 20 July 2012
Available online 2 August 2012

Keywords:
Liquid/solid interface
Thermostat effects
Thermal resistance
Kapitza resistance
Kapitza length

ABSTRACT

Molecular Dynamics simulations of heat conduction in liquid Argon confined in Silver nano-channels are performed subject to three different thermal conditions. Particularly, different surface temperatures are imposed on Silver domains using a thermostat in all and limited number of solid layers, resulting in heat flux in the liquid domain. Alternatively, energy is injected and extracted from solid layers to create a NVE liquid Argon system, which corresponds to heat flux specification. Imposition of a constant temperature region in the solid domain results in an unphysical temperature jump, indicating the presence of an artificial thermal resistance induced by the thermostat. Thermal resistance analyses for the components of each case are performed to distinguish the artificial and interface thermal resistance effects. Constant wall temperature simulations are shown to exhibit superposition of the artificial and interface thermal resistance values at the liquid/solid interface, while applying thermostat on wall layers sufficiently away from the liquid/solid interface results in consistent predictions of the interface thermal resistance. Injecting and extracting energy from each solid layer eliminates the artificial resistance. However, the method cannot directly specify a desired temperature difference between the two solid domains.

1. Introduction

Miniaturization of microelectronic device components and the development of nano-electro-mechanical systems require advanced understanding of thermal transport in nano-materials and devices, where the atomic nature of matter becomes important and the validity of well-known continuum approximations becomes questionable [1]. As a result, heat transfer in nanostructures and channels are modeled using molecular dynamics (MD) method [2,3]. The most widely used approach to create a heat flux in the domain is to employ thermostats to regulate the temperature in hot and cold regions, while utilizing a thermostat free zone in the middle. The thermostat applied regions often utilize the velocity rescaling, Nose-Hoover or Langevin thermostats [4]. Each of these algorithms constrains the temperature based on the kinetic energy of atoms. Many MD based heat conduction studies for homogenous solid domains report emergence of an *artificial thermal resistance* (i.e., temperature jump) at the interface of the thermostat applied and thermostat free regions [5–14]. Phonon transport in solids arises from long term correlated motion between neighboring atoms. Thermostat applies a random force to the atoms to keep them at the prescribed temperature. This de-correlates the motion between atoms at the interface of the thermostat applied and thermostat free regions, and leads to lower thermal conductivity with an *artificial interface resistance*. Although this phenomenon has been widely observed in solid systems, its significance at the liquid/solid interface is largely unknown.

* Corresponding author. Tel.: +1 757 683 6818.
E-mail address: abeskok@odu.edu (A. Beskok).

0021-9991/$ - see front matter © 2012 Elsevier Inc. All rights reserved.
http://dx.doi.org/10.1016/j.jcp.2012.07.026

Thermal transport through an interface between two dissimilar materials results in a temperature jump ΔT due to the mismatch in phonon spectrum of the materials forming the interface. For given a heat flux $\vec{j}$, this jump can be associated with an *interfacial thermal resistance* (R_K), known as the Kapitza resistance [15]:

$$\Delta T = -R_K \vec{j} \cdot \vec{n}, \tag{1}$$

where $\vec{n}$ is the outward unit normal from the wall. Alternatively it is possible to define a thermal resistance (Kapitza) length (L_K), by extrapolating the temperature profile from liquid in to the solid, where the wall temperature is reached. The Kapitza length can be predicted using,

$$\Delta T = L_K \left.\frac{\partial T}{\partial n}\right|_{\text{liquid}}, \tag{2}$$

where $\partial T/\partial n$ is the thermal gradient on the liquid side, and $\Delta T = T_{\text{liquid}} - T_{\text{wall}}$. It is crucial to realize that Eq. (2) requires onset of continuum behavior where a local temperature profile can be defined. This condition can also be used as a Navier-type boundary condition in solution of continuum-based heat transfer equations. Kapitza resistance (R_K) can be related with the Kapitza length (L_K) using Eqs. (1) and (2), and Fourier law of heat conduction. Recent MD studies of nano-scale heat conduction in simple (Lenard-Jones) fluids have shown emergence of continuum behavior, and the validity of Fourier law in channels with dimensions as small as ten molecular diameters (≈3.5 nm) [16,17]. Utilization of continuum-based models requires a priori knowledge of the Kapitza length (L_K) for specific liquid/solid interfaces, where Eq. (2) serves as the proper temperature jump boundary condition. Such continuum approach will allow simulation of vast number of heat transport problems in industrially relevant sized (∼ 1 m) complex geometries for sufficiently long time-scales (∼1 day), which is impossible to achieve using molecular simulation methods. Due to its potential impacts, there have been recent attempts to characterize the Kapitza length at liquid/solid interfaces using molecular dynamics method [18,19]. Most of these approaches sandwiched a liquid domain between two solid walls, and induced heat flux by fixing the wall temperatures using a thermostat. As a result, effects of the artificial thermal resistance were carried onto the liquid/solid interface.

In this study, we investigate heat conduction through the liquid Argon – solid Silver interface using non-equilibrium molecular dynamics simulations by employing three different thermal boundary treatments. Our *objectives* are to investigate the effect of this *artificial thermal resistance* and distinguish it from the actual Kapitza resistance at the liquid/solid interface. In order to achieve these goals, we present heat conduction results in the solid-liquid-solid domains obtained by applying Langevin thermostat to all wall layers; only to a small number of wall layers that are sufficiently away from the liquid/solid interface; and by injecting and removing energy from the wall layers. All results are organized to characterize the artificial thermal resistance, Kapitza resistance and length using simple heat conduction analysis. Results of systematic studies obtained by varying the wall temperatures are also presented.

2. Three-dimensional MD simulation details

We studied liquid Argon confined between two parallel solid Silver walls by using LAMMPS (Large-scale Atomic/Molecular Massively Parallel Simulator), a molecular dynamics code from Sandia National Laboratories [20]. Fig. 1 illustrates a snapshot of the simulation domain. Total dimensions in longitudinal (x), vertical (y), and lateral (z) directions are 16.4, 3.7 and 3.7 nm, respectively. The domain was constructed using 1830 Argon and 7776 Silver molecules. The first Silver

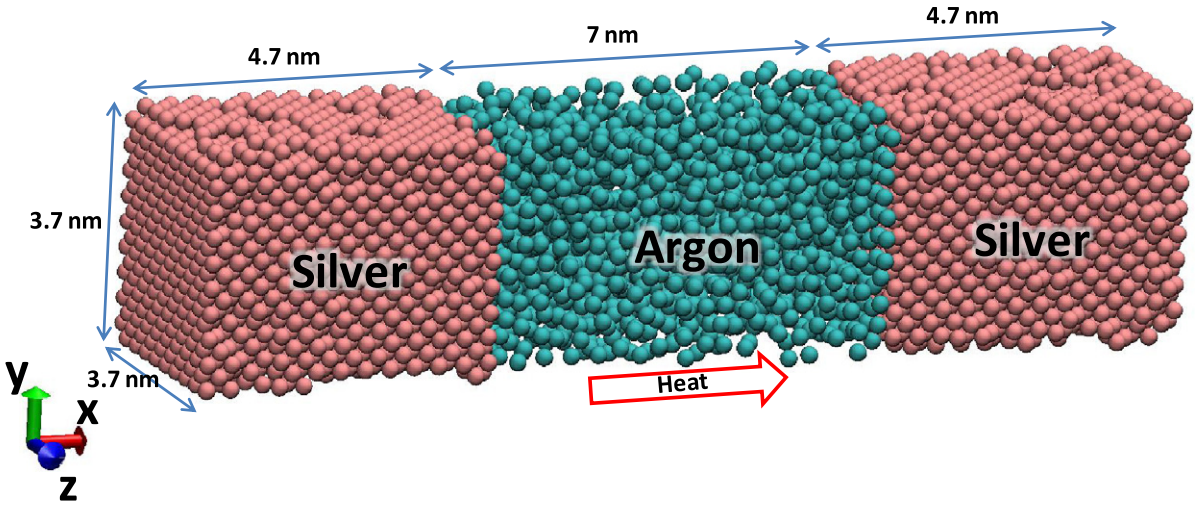

Fig. 1. Snapshot of the MD simulation domain with domain size.

domain lies between 0 and 48 Å, and the second Silver domain is from 118 Å to 166 Å, while the liquid Argon is confined to 70 Å spacing between the two walls. The corresponding number density of Argon is $\rho = 0.8$ ($\#\sigma^3\,\mathrm{nm}^{-3}$). The walls on each side of the domain contain 24 Silver layers that are 0.2043 nm apart from each other. Each Silver layer contains 162 molecules resulting in number density of 5.7 ($\#\sigma^3\,\mathrm{nm}^{-3}$). Periodic boundary conditions are applied in the vertical (y) and lateral (z) directions. Silver walls are modeled as face-centered cubic (FCC) structures with (0,0,1) crystal plane facing the fluid. Atoms in the outmost layer of both Silver walls are fixed to their original locations to maintain a fixed volume system, while the remaining atoms throughout the domain are free to move.

Mass for an Argon molecule is $m = 6.63 \times 10^{-26}$ kg, its molecular diameter is $\sigma = 0.3405$ nm and the depth of the potential well for Argon is $\varepsilon = 119.8 \times k_b$. Lenard-Jones (L-J) 6–12 potential was utilized to model the van der Waals interactions between Argon–Argon and Argon–Silver molecules with a cutoff distance of 1 nm. The truncated (6–12) Lennard-Jones (L-J) potential is given as,

$$\Phi_{\text{truncated}}(r_{ij}) = 4\varepsilon\left(\left(\left(\frac{\sigma}{r_{ij}}\right)^{12} - \left(\frac{\sigma}{r_{ij}}\right)^{6}\right) - \left(\left(\frac{\sigma}{r_c}\right)^{12} - \left(\frac{\sigma}{r_c}\right)^{6}\right)\right), \tag{3}$$

where r_{ij} is the intermolecular distance, ε is the depth of the potential well, σ is the molecular diameter and r_c is the cut-off radius [4]. Lorentz-Berthelot mixing rule is employed to calculate the Lennard-Jones parameters for Argon–Silver interactions [21]. MD parameters utilized for Argon–Argon and Argon–Silver interactions are presented in Table 1. Silver-Silver interactions are calculated using the *embedded atom method* (*EAM*) which is a many-body potential for slightly more computational cost than the pair potential, and works especially well for FCC structures [22,23].

Simulations are started from the Maxwell–Boltzmann velocity distribution for all molecules at 115 K. Initial particle distribution is evolved 10^6 time-steps (4 ns) to reach an isothermal steady state using 4 fs time steps. During this process, the Nose-Hoover thermostat is applied to the molecules to maintain the system's temperature at 115 K. Afterwards, temperatures of the Silver walls are modified to serve as heat baths to induce heat flux through the liquid/solid interfaces. At the same time, NVE ensemble is applied to liquid Argon domain. Simulations are performed for an additional 10^6 time-steps (4 ns) to ensure that the system attains equilibrium in presence of the heat flux. After which, time averaging of desired properties are performed for 2×10^6 additional time steps (8 ns). Longer time averaging has also been performed to confirm the convergence of density and temperature profiles to steady state.

Two different heat bath techniques are employed to investigate their effects. First, a constant surface temperature is maintained using Langevin thermostat. Langevin damping factor is taken to be 0.1 ps which is prescribed by the phonon frequency of solid silver ($f_D = 0.223$ ps) at Debye temperature of $T_D = 215$ K [24,25]. Different wall temperatures are assigned to create heat flux through the liquid/solid interfaces. Langevin technique is employed as a global thermostat on the specified number of solid layers for each case. Second, a constant heat flux is obtained by injecting and removing energy through the heat baths to support a temperature gradient across the system. The simulated cases are summarized in Table 2. The computational domain is divided into 200 slab bins with the size of 0.083 nm. In order to interpret the temperature profiles obtained using fine-bins, we also obtained temperature distribution using 20 slab bins. Temperature profiles from the fine and coarse bin cases were consistent, and showed that local thermal equilibrium is reached in the simulations using fine bins. Coarse bin results are omitted for brevity of this work. Achievement of local thermal equilibrium in such nano-scale confined domains was addressed earlier in [16,17].

Irving–Kirkwood (I–K) expression is utilized to compute the heat flux vector for an N particle system using unity differential operator approximation as follows [26,27],

$$J_k = \frac{1}{\text{Vol}}\left\langle \sum_{i}^{N} V_k^i (E^i + \Phi^i) + \sum_{i,j}^{N} (r_k^j + r_k^i) W^{i,j} \right\rangle, \tag{4}$$

$$E^i = \frac{1}{2} m^i ((V_x^i)^2 + (V_y^i)^2 + (V_z^i)^2), \tag{5}$$

$$W^{i,j} = \frac{1}{2}(V_x^i f_x^{i,j} + V_y^i f_y^{i,j} + V_z^i f_z^{i,j}), \tag{6}$$

where the first term on the right hand side of Eq. (4) is the kinetic and potential energies carried by particle i, and the second term is the energy transfer to particle i by force interactions with the surrounding particles. In the first term, V_x^i is the peculiar velocity component of particle i in k-direction, while k is the axes of the Cartesian coordinate system; E^i is the kinetic

Table 1
Intermolecular interaction parameters for Argon-Argon and Argon–Silver molecules.

Molecule couple	σ (Å)	ε (eV)	$\varepsilon/\varepsilon_{Ar}$
Ar–Ar	3.405	0.01	1
Ar–Ag	2.978	0.06	6

Table 2
Kapitza lengths (L_k) at hot and cold surfaces, heat flux, temperature gradients and thermal conductivity of liquid Argon for six different cases.

Case #	Description	Heat flux (W/m^2)	$dT/dx\|_{liquid}$ (K/Å)	k (mW/Km)	L_k Hot (Å)	@T_w (K)	L_k Cold (Å)	@T_w (K)
Case 1	140–90 K 23 lys	6.01×10^8	0.579	103.9	11.1	140.0	9.4	90.0
Case 2	140–90 K 3 lys	5.91×10^8	0.576	102.6	5.8	136.8	3.1	92.7
Case 3	136.8–92.7 K 23 lys	5.31×10^8	0.509	102.2	11.6	136.8	9.7	92.7
Case 4	136.8–92.7 K 3 lys	5.2×10^8	0.511	104.0	5.3	134.4	3.5	95.1
Case 5	Add heat 3 lys of 24 lys	6.36×10^8	0.620	102.6	5.9	139.8	3.0	90.9
Case 6	Add heat 3 lys of 4 lys	6.44×10^8	0.624	103.2	6.0	142.1	3.1	93.2

and Φ^i is the potential energy of particle i calculated using Eqs. (5) and (3), respectively. In the second component of Eq. (4), $(r_k^j - r_k^i)$ is the kth component of the relative distance vector between particles i and j. The $W^{i,j}$ term is given in Eq. (6), where $f_l^{i,j}$ is the intermolecular force exerted on particle i by particle j in the Cartesian coordinate direction l.

3. Results

In this section, we present MD simulation results for heat conduction in Silver–Argon–Silver system subjected to three different thermal conditions. Particularly a constant surface temperature is imposed via a thermostat in all and limited number of wall layers and energy is injected and removed from each solid layer. The latter corresponds to the specification of heat flux in the domain. Thermal resistance values for each case are considered separately to distinguish the artificial thermal resistance and Kapitza resistance effects on liquid/solid interfaces.

3.1. Constant surface temperature

Case 1 utilizes constant temperature surfaces, where all 23 Silver layers of the left and right surfaces are maintained at 140 K and 90 K, respectively using a Langevin thermostat. The number density profile shown in Fig. 2 illustrates the system consisting of three distinct domains. Argon density exhibits strong near wall layering due to the wall force field effects and local Argon-Argon interactions [28]. The density layering extends approximately 2 nm from each surface, after which the liquid Argon density reaches nearly a constant value of 0.8 (#σ^3 nm^{-3}). Slight density variation in this bulk liquid region is due to the temperature gradient, where the Argon density increases with decreased temperature. Local Argon density near the high temperature (left) wall is less than that near the low temperature (right) wall. Argon density fluctuates severely near the surface, resulting in nearly zero molecules within certain bins. Depletion of Argon molecules near the surfaces has profound effects on the definition of local liquid temperature. Very few liquid molecules are present at these density minima, where local temperature cannot be defined accurately. In order to address this problem we omitted presentation of temperature in these "empty" bins as can be observed from the near wall temperature profiles.

Fig. 2 also shows the temperature profiles obtained using 200 slab bins. While the Silver surfaces are kept at constant temperatures, liquid Argon temperature varies linearly in bulk of the nano-channel. Temperature jumps at the liquid/solid

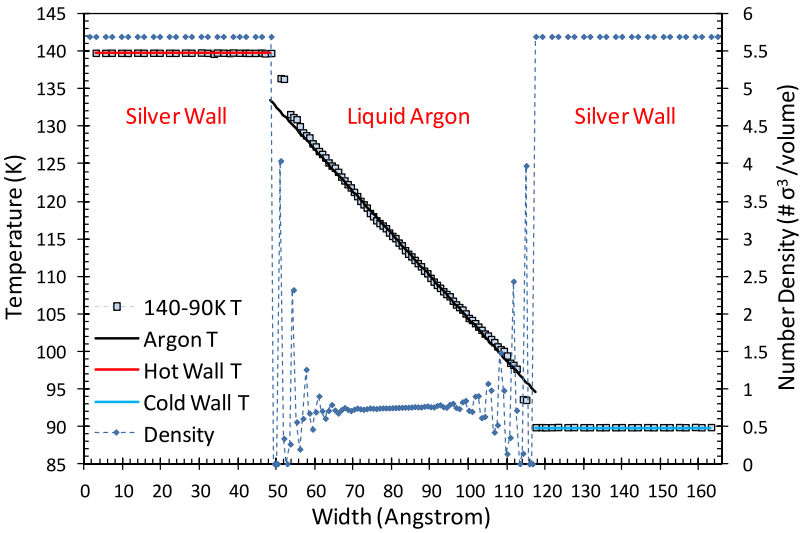

Fig. 2. Temperature (left axis) and density (right axis) profiles of liquid Argon confined between 24 layer Silver walls. Langevin thermostat is applied onto 23 layers of each Silver wall separately to maintain them at 140 K and 90 K (Case 1).

interfaces are apparent in the results. Extrapolations of the liquid temperature on to the walls reveal discontinuities between the extrapolated fluid temperature and wall temperature. These temperature jumps are due to the Kapitza resistance (R_K), and can be related to the Kapitza length (L_k) using Eqs. (1) and (2). In order to characterize the temperature distribution in the bulk of liquid Argon, we performed linear least square fits to the MD data, and measured sum of the squares of the residual, which is a measurement of how well the least square fit represents the data. The values are all below 1%, indicating that the temperature profile is linear in the bulk of the channel. Slight curvature in the temperature profile can be attributed to the temperature dependence of Argon's thermal conductivity. Surprisingly, linear temperature profiles are observed up to the second Argon-density peak, approximately 0.5 nm from the Silver wall. Hence, strong density fluctuations do not significantly affect the temperature profile beyond 0.3 nm from each wall. In addition, the fine bin temperature distribution in liquid Argon near the Silver surface, especially within the first density peak near the walls, shows steep temperature variations compared to the bulk region. This behavior can be attributed to strong interactions of the Silver–Argon molecules.

Next, we calculate the Kapitza length, L_k, by using Eq. (2). First we obtained the local temperature gradient from the MD results, and matched this with the slope of the linear curve fits to the temperature profiles in the bulk of the channel. Then, we extrapolated the liquid temperature onto the solid surface, which was assumed to be the center of the last Silver layer facing the liquid; and calculated the local temperature jump ($\Delta T = T_{\text{liquid}} - T_{\text{wall}}$). As suggested by Eq. (2), this temperature jump and the linear slope of Argon temperature profile yield the value of L_K. In the current case, when thermostat is applied to all 23 Silver layers, L_k of Argon/Silver interface is 11.1 Å and 9.4 Å at the hot (140 K) and cold (90 K) surfaces, respectively (Table 2). These results clearly indicate the temperature dependence of L_k. In the mean time, we also calculated the heat flux using Eq. (4), and utilized the temperature gradient obtained from MD result to calculate the thermal conductivity using Fourier law. Thermal conductivity for liquid Argon at average temperature of 115 K is 103.9 mW/mK, which matches the published bulk values well [29,30]. The calculated Kapitza lengths, heat flux, temperature gradients and thermal conductivity of liquid Argon are tabulated in Table 2.

In order to investigate the thermostat effects, we created Case 2 by applying the Langevin thermostat to the outer most second, third and fourth layers of the left and right Silver slabs (note that the outer first layer of each wall is fixed to define a constant simulation volume). As a result, the remaining 20 Silver layers are left to interact freely to develop their own temperature profile based on phonon scattering of Silver surfaces. By considering that the wall layers are 0.2043 nm apart from each other, 20 Silver layers separate the thermostated molecules from the liquid/solid interface by approximately 15 atomic spacing. Such large distances minimize the thermostat effects at the liquid/solid interface. Fig. 3 shows the temperature profile for Case 2. Sudden temperature drops at the interface of the thermostat applied and thermostat free regions are observed inside the Silver domains. This is due to the dynamic rescaling of thermostat, which results in phonon mismatch at this interface. Further insight regarding to this behavior may be obtained by considering the Green–Kubo formula [31,32], which is widely used to calculate the thermal conductivity from equilibrium simulations. Assuming local equilibrium, conductivity (k_j) between slices j and $j+1$, is proportional to the long-time average of the heat flux autocorrelation given as,

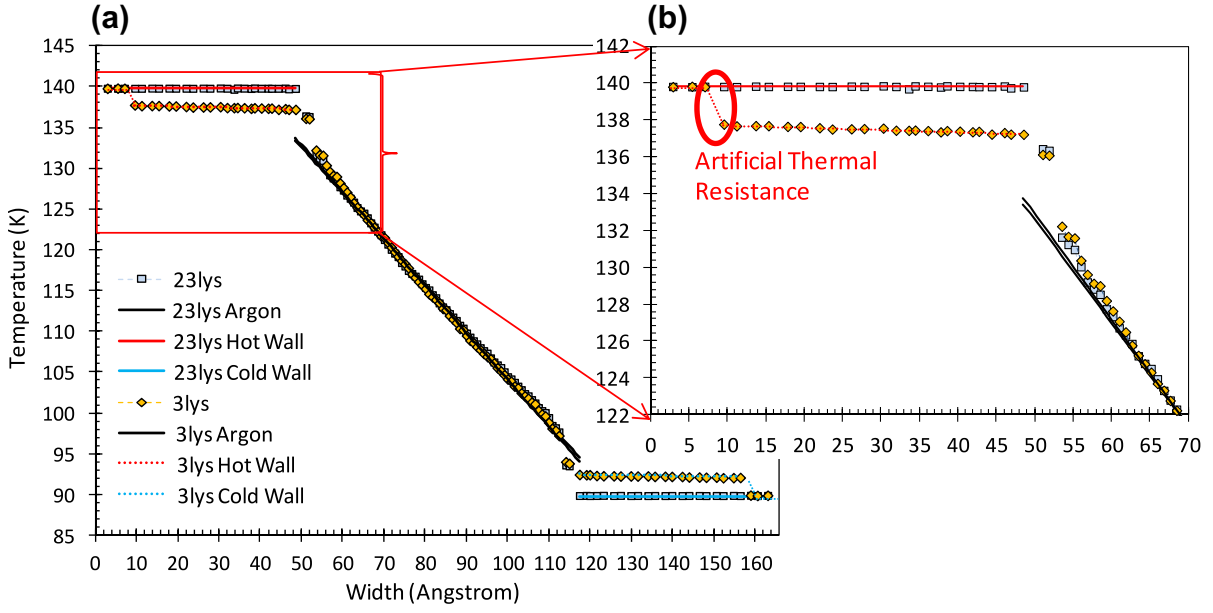

Fig. 3. Temperature profile when Langevin thermostat is applied on three layers of Silver walls to keep them at 140 K and 90 K, respectively (Case 2). Result for Case 1 is also shown for comparison (a). Zoomed view of the hot surface shows presence of an artificial thermal resistance at the interface of the thermostat applied and thermostat free regions of the solid domain (b).

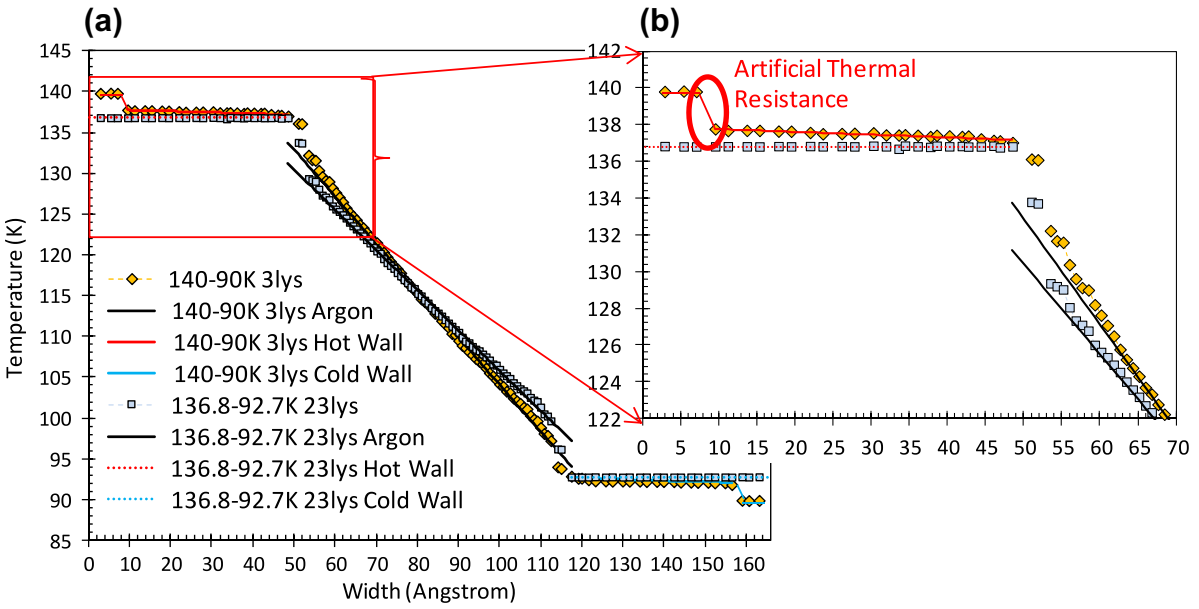

Fig. 4. Temperature profile when Langevin thermostat is applied on 23 layers of each silver wall domain to keep them at 136.8 K and 92.7 K, respectively (Case 3). Result for Case 2 is also shown for comparison (a). Zoomed view of the hot surface shows that both simulations yield identical wall temperatures at the liquid/solid interface (b).

$$k_j \approx \lim_{t\to\infty} \int_0^t \langle q_j(s) q_j(0) \rangle ds, \tag{7}$$

where $q_j(t)$ is the instantaneous net heat flux between slices j and $j+1$, developed due to long-term correlations of the particle interactions. Any thermostat altering particle motions corrupts this autocorrelation by reducing the thermal conductivity at the interface of the thermostat applied region. This implies that the Langevin thermostat leads to reduced conductivity between the thermostat applied and thermostat free Silver layers, and creates an *artificial thermal resistance*. Similar behavior has also been consistently observed for different thermostat techniques with different amounts of temperature jumps.

Fig. 3 (right) shows zoomed view of the temperature distribution in Silver. After the temperature jump due to the artificial thermal resistance, Silver temperature is reduced linearly to 136.8 K at the Argon/Silver interface. This reduction in Silver temperature is due to heat flux through the solid wall. Similar to the hot wall, the cold wall also experiences a temperature jump, flowed with linear increase in Silver temperature to 92.7 K. Linear least square fits to Silver and Argon temperatures result in good fits with measured sum of the squares of the residual lower than 1%. We must note that MD simulations here consider only the intramolecular vibrational energy transfer, while thermal transport in metals is dominated by electron interactions. As a result, calculated thermal conductivity of Silver is less than the reported bulk material values. Despite this limitation, Silver blocks serve as heat baths to induce heat flux on the Argon/Silver interfaces. Because of the definitions of the Kapitza resistance and Kapitza length given in Eqs. (1) and (2), heat transfer in Silver domains has negligible effects on our investigation. Similar to the earlier calculations, L_k is found by using Eq. (2). Extrapolation of Argon temperature onto the center of the last Silver layer facing liquid Argon enabled us to calculate the local temperature jump ($\Delta T = T_{\text{fluid}} - T_{\text{wall}}$), thus the value for L_K. When thermostat is applied only to the outer three layers of Silver walls, L_k at the Argon/Silver interface is found to be 5.8 Å and 3.1 Å on the hot (136.8 K) and cold (92.7 K) surfaces, respectively (Table 2). Values of the Kapitza length are approximately half of the values calculated in Case 1. This proves the thermostat effect on the Silver/Argon interface. Interestingly, the calculated heat flux values for both cases are almost identical (Table 2) revealing that the total thermal resistance of the simulation system is approximately kept constant regardless of the location where the thermostat is applied. Slight reduction in the heat flux in Case 2 is due to heat conduction in Silver slabs.

In order to validate our observations regarding the thermostat effect on L_k, we conducted additional investigations. In Case 3, we applied constant temperature on Silver walls using a thermostat, by keeping the walls at 136.8 K and 92.7 K so that the wall temperature at the liquid/solid interface is the same with Case 2. Temperature profile for Cases 2 and 3 are shown in Fig. 4. Despite the identical interface wall temperatures, Argon temperature variation and the heat flux in these two systems are different. The L_k values for Case 2 are 11.6 Å and 9.7 Å at the 136.8 K and 92.7 K surfaces, respectively, which are values closer to L_k prediction for Case 1 (Table 2). Case 4 was created by applying thermostat to the outermost three wall layers to keep them at 136.8 K and 92.7 K. This case matches the temperature difference imposed in Case 3 ($\Delta T = 44.1$ K). As a result, heat flux values in Cases 3 and 4 are similar, indicating that the total thermal resistances of these two cases are the

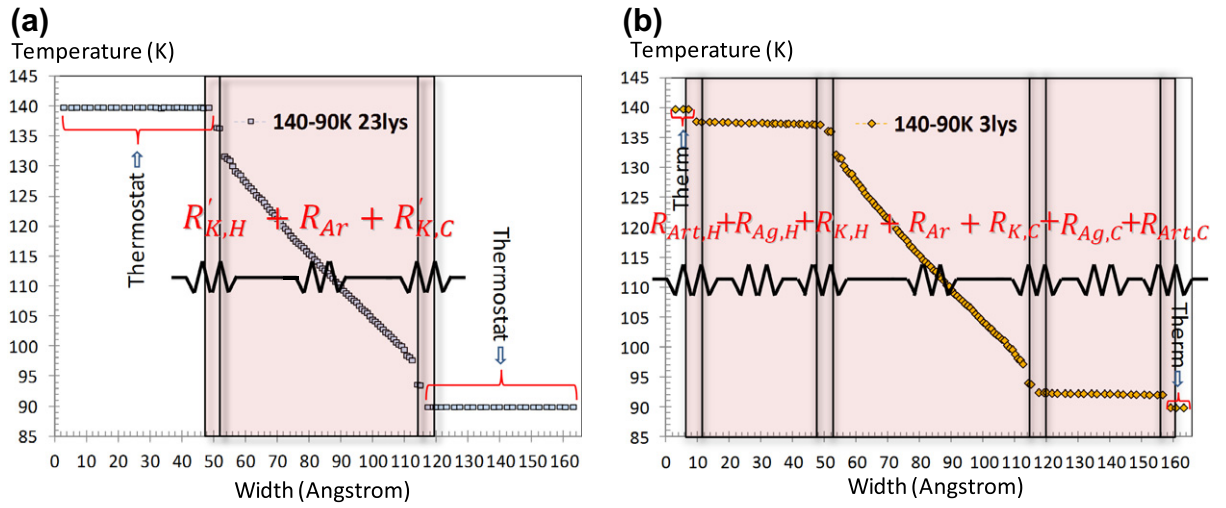

Fig. 5. Temperature profiles and the corresponding thermal resistances in the simulation domains when the thermostat is applied on all (a), and three outermost wall layers (b).

same independent of the location of thermostat. However, calculated L_k values for Case 4 in Table 2 are half of the values calculated for Case 3, and it is closer to the predictions in Case 2.

3.2. Calculation of the thermal resistance values

According to the Fourier law for steady-state heat conduction, the overall heat flux across a system of composite slabs with different thermal conductivities can be written as,

$$q = (T_{\mathrm{Hot}} - T_{\mathrm{Cold}})\frac{1}{R_{\mathrm{Tot}}}, \tag{8}$$

where T_{Hot} and T_{Cold} are the temperature of the cold and hot reservoirs, respectively, while R_{Tot} is the total thermal resistance of the system. For Cases 1 and 3, the total thermal resistance of system can be written as,

$$R'_{\mathrm{Tot}} = R'_{\mathrm{K,H}} + R_{\mathrm{Ar}} + R'_{\mathrm{K,C}}, \tag{9}$$

where $R'_{\mathrm{K,H}}$ and $R'_{\mathrm{K,C}}$ are the interfacial thermal resistances of two Argon/Silver interfaces on the hot and cold sides, respectively; and R_{Ar} is the thermal resistance of liquid Argon in middle of the channel (Fig. 5a). We must note that the thermal resistance of the domains utilizing a thermostat is zero. The total thermal resistance of the system as well as the thermal resistance of each part can be calculated by considering heat flux and the temperature jump using $R_i = \Delta T_i/q$, where i indicates the corresponding section(s) of the domain. The thermal resistance values are tabulated in Table 3. Using a similar description, the total thermal resistance for Cases 2 and 4 consists of seven different thermal resistance parts (Fig. 5b), which can be written as

$$R_{\mathrm{Tot}} = R_{\mathrm{Art,H}} + R_{\mathrm{Ag,H}} + R_{\mathrm{K,H}} + R_{\mathrm{Ar}} + R_{\mathrm{K,C}} + R_{\mathrm{Ag,C}} + R_{\mathrm{Art,C}}, \tag{10}$$

where $R_{\mathrm{Art,H}}$ and $R_{\mathrm{Art,C}}$ are the *artificial thermal resistances* of two regions at the interface of the thermostat applied and thermostat free regions; $R_{\mathrm{Ag,H}}$ and $R_{\mathrm{Ag,C}}$ are the thermal resistances due to the thermal conductivities of two (thermostat free) Silver layers on the left and right, and $R_{\mathrm{K,H}}$ and $R_{\mathrm{K,C}}$ are the *interface thermal resistances*. Thermal resistances of these seven different layers are calculated using $R_i = \Delta T_i/q$ and their values are tabulated in Table 3.

It is important to notice that the total temperature drop in Cases 1 and 2 are identical, while the total heat flux in Case 1 is slightly higher than that in Case 2 (Table 2). As a result, the total thermal resistance in Case 1 is lower than the total resistance in Case 2. The difference between the two total resistance values is due to heat conduction in solid slabs in Case 2. If we remove the resistance added by the solid slabs, which is approximately 1.9% of R_{Tot}, the total thermal resistance values for Cases 1 and 2 becomes similar. As the liquid Argon resistance is the same for both cases, interfacial thermal resistances calculated in Case 1 are equal to the sum of the *interface thermal resistances* and *artificial thermal resistances* in Case 2.

$$R'_{\mathrm{K,H}} = R_{\mathrm{Art,H}} + R_{\mathrm{K,H}}, \qquad R'_{\mathrm{K,C}} = R_{\mathrm{Art,C}} + R_{\mathrm{K,C}}. \tag{11}$$

This discussion consistently applies to the Cases 3 and 4, as can be seen in the individual resistance values in Table 3. Therefore Eq. (11) clearly explains the thermostat effect on thermal resistance calculations at an interface. The L_k value calculated near a thermostat applied surface leads to wrong predictions, since it takes into account the *artificial thermal resistance* created by the thermostat.

Table 3
Thermal resistance components of the domain for six different simulation cases.

Case #	Description	Flux (W/m^2)			$R'_{K,H}$ ($K\,m^2/W$)	R_{Ar} (Km^2/W)	$R'_{K,C}$ ($K\,m^2/W$)			R'_{Tot} ($K\,m^2/W$)
1	140–90 K 23 lys	6.01×10^8			9.5×10^{-9}	66.9×10^{-9}	6.7×10^{-9}			83.1×10^{-9}
3	136.8–92.7 K 23 lys	5.31×10^8			9.4×10^{-9}	67×10^{-9}	6.6×10^{-9}			83×10^8
	Description	Flux (W/m^2)	$R_{Art,H}$ ($K\,m^2/W$)	$R_{Ag,H}$ ($K\,m^2/W$)	$R_{K,H}$ ($K\,m^2/W$)	R_{Ar} (W/m^2)	$R_{K,C}$ ($K\,m^2/W$)	$R_{Ag,C}$ ($K\,m^2/W$)	$R_{Art,C}$ ($K\,m^2/W$)	R_{Tot} ($K\,m^2/W$)
2	140–90 K 3 lys	5.91×10^8	4×10^{-9}	0.8×10^{-9}	5.4×10^{-9}	67×10^{-9}	2.7×10^{-9}	0.8×10^{-9}	3.9×10^{-9}	84.6×10^{-9}
4	136.8–92.7 K 3 lys	5.2×10^8	4.1×10^{-9}	0.8×10^{-9}	5.3×10^{-9}	67.1×10^{-9}	2.6×10^{-9}	0.9×10^{-9}	4×10^{-9}	84.8×10^8
	Description	Flux (W/m^2)		$R_{Ag,H}$ ($K\,m^2/W$)	$R_{K,H}$ ($K\,m^2/W$)	R_{Ar} (W/m^2)	$R_{K,C}$ ($K\,m^2/W$)	$R_{Ag,C}$ ($K\,m^2/W$)		R_{Tot} ($K\,m^2/W$)
5	Add heat 3 lys of 24 lys	6.36×10^8		1.7×10^{-9}	6.1×10^{-9}	67.6×10^{-9}	3.3×10^{-9}	1.8×10^{-9}		80.5×10^8
6	Add heat 3 lys of 4 lys	6.44×10^8		0.6×10^{-9}	6.2×10^{-9}	66.4×10^{-9}	3.2×10^{-9}	0.4×10^{-9}		76.8×10^8

Further studies are conducted to investigate the effect of assigned wall temperature on the *artificial thermal resistance*. We performed a series of simulations by fixing one surface temperature and varying the temperature difference. First, we fixed the left wall temperature at 140 K and gradually increased the right wall temperature form 90 K to 120 K (Fig. 6a). Then, we fixed the right wall temperature at 90 K and gradually decreased the left wall temperature from 140 K to 110 K (Fig. 6b). These simulations result in different heat flux values and temperature gradients. Thermal resistance of each part is calculated by considering the heat flux and temperature jump of the corresponding component using $R_i = \Delta T_i/q$ and the results are shown in Table 4. Fig. 6 shows that the temperature jumps at the Silver/Argon, and thermostat applied and thermostat free regions decrease with decreased temperature difference. This is also accompanied with a reduction in heat flux. Since thermal resistance is the ratio of the temperature jump to heat flux, values of the thermal resistance are independent of the temperature differences. Total thermal resistance of the system shows variations due to the change in thermal conductivity as a function of average domain temperature. Thermal conductivity increases with increased temperature, thus the total resistance decreases from 87.6 to 81.6×10^{-9} K m^2/W. Thermal resistance of liquid Argon shows clear dependence on average Argon temperature due to the variations in Argon conductivity. While the average temperature in the channel changes from 130 K to 100 K, the liquid Argon resistance changes from 65.7 to 69.2×10^{-9} Km^2/W. The interface thermal resistance is also affected by the local temperature, which varies from 3.9 to 5.4×10^{-9} K m^2/W at hot ($\leqslant$140 K) surfaces, and from 3.8 to 4.1×10^{-9} Km^2/W at cold ($\geqslant$90 K) surfaces. Thermal resistance of solid Silver slabs is nearly a constant at 0.8 to 0.9×10^{-9} K m^2/W. Our main focus is the behavior of the *artificial thermal resistance*, which shows small temperature dependency, and varies between 3.9 and 4.2×10^{-9} K m^2/W.

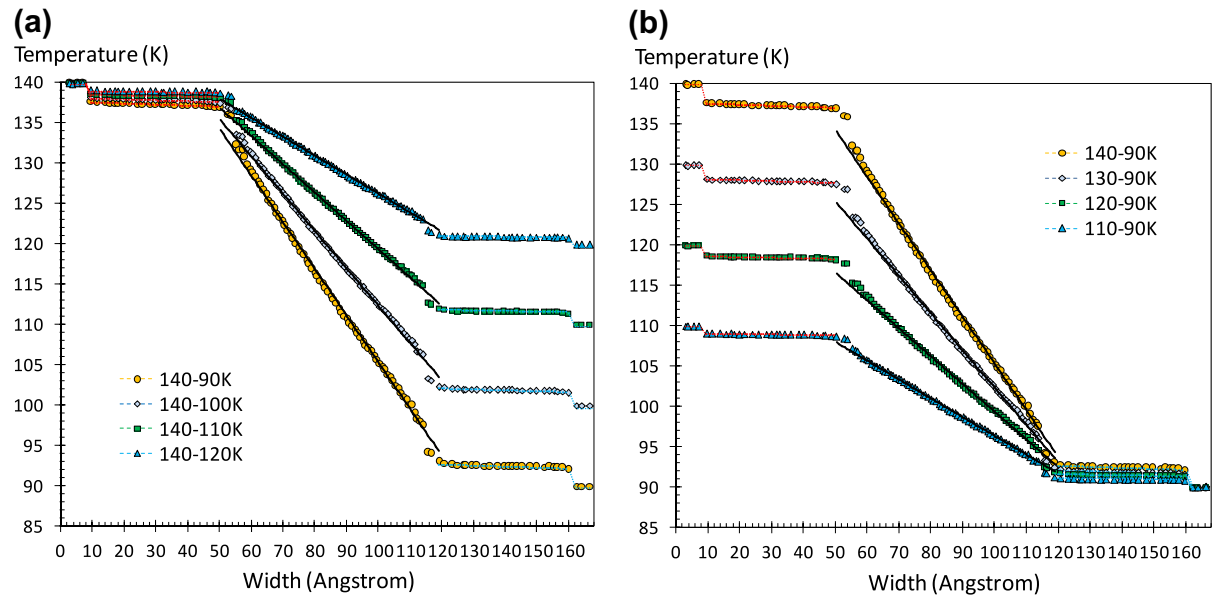

Fig. 6. Temperature profiles when Langevin thermostat is applied on three outermost layers of Silver walls to keep them at different temperatures. Hot wall temperature is fixed at 140 K while cold wall temperature is varied (a). Cold wall temperature is fixed at 90 K while hot wall temperature is varied (b).

Table 4
Thermal resistance components of the domain, when thermostat is applied on three outermost Silver layers of the walls to keep the left surface at 140 K and right surface at 90, 100, 110 and 120 K. Similar data for cases where the right wall is kept at 90 K and the left wall temperature is varied between 140, 130, 120 and 110 K.

Case	Flux (W/m^2)	$R_{Art,H}$ (Km^2/W)	$R_{Ag,H}$ (Km^2/W)	$R_{K,H}$ (Km^2/W)	R_{Ar} (W/m^2)	$R_{Ag,C}$ (Km^2/W)	$R_{K,C}$ (Km^2/W)	$R_{Art,C}$ (Km^2/W)	R_{Tot} (Km^2/W)
140–90 K	5.91×10^8	4×10^{-9}	0.8×10^{-9}	5.4×10^{-9}	67×10^{-9}	2.7×10^{-9}	0.8×10^{-9}	3.9×10^{-9}	84.6×10^{-9}
140–100 K	4.76×10^8	4.2×10^{-9}	0.9×10^{-9}	4.7×10^{-9}	66.8×10^{-9}	2.6×10^{-9}	0.9×10^{-9}	3.9×10^{-9}	84×10^{-9}
140–110 K	3.63×10^8	4.1×10^{-9}	0.8×10^{-9}	4×10^{-9}	66.4×10^{-9}	2.3×10^{-9}	0.8×10^{-9}	4.1×10^{-9}	82.5×10^{-9}
140–120 K	2.45×10^8	4.2×10^{-9}	0.8×10^{-9}	3.9×10^{-9}	65.7×10^{-9}	2.2×10^{-9}	0.8×10^{-9}	4×10^{-9}	81.6×10^{-9}
140–90 K	5.91×10^8	4×10^{-9}	0.8×10^{-9}	5.4×10^{-9}	67×10^{-9}	2.7×10^{-9}	0.8×10^{-9}	3.9×10^{-9}	84.6×10^{-9}
130–90 K	4.73×10^8	4.1×10^{-9}	0.9×10^{-9}	5.2×10^{-9}	67.3×10^{-9}	2.8×10^{-9}	0.9×10^{-9}	3.8×10^{-9}	85×10^{-9}
120–90 K	3.51×10^8	4.2×10^{-9}	0.9×10^{-9}	5.4×10^{-9}	67.5×10^{-9}	2.9×10^{-9}	0.8×10^{-9}	3.9×10^{-9}	85.6×10^{-9}
110–90 K	2.28×10^8	4.2×10^{-9}	0.9×10^{-9}	5.4×10^{-9}	69.2×10^{-9}	3.1×10^{-9}	0.8×10^{-9}	4×10^{-9}	87.6×10^{-9}

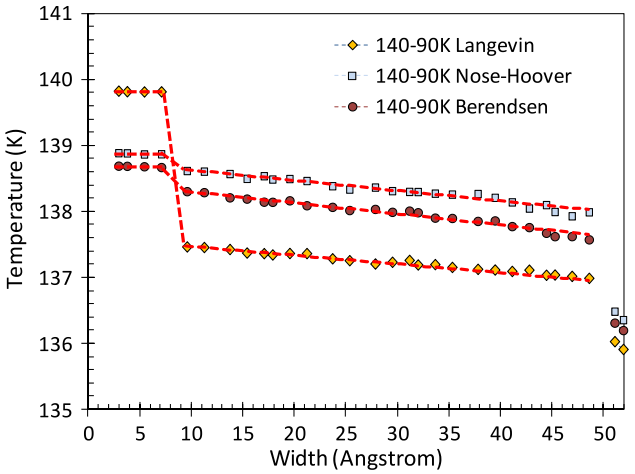

Fig. 7. Temperature profiles of different thermostat techniques resulting in different artificial thermal resistance values between the thermostat applied and thermostat free Silver layers.

In addition to the presented results of the Langevin thermostat, we also studied the current simulation domain using different thermostat techniques. Fig. 7 shows temperature profiles of the hot reservoir using Langevin, Berendsen [33] and Nose-Hoover [34] thermostats applied to Case 2. Different from the Langevin case, applying Berendsen and Nose Hoover on multiple silver layers create temperature gradient inside the thermostat applied region different than the temperature gradient of the thermostat free domain, complicating analysis of the artificial resistance. Applying Berendsen and Nose Hoover thermostats on each layer separately mimics an isothermal system similar to the Langevin case. By this approach the artificial thermal resistance is carried on to the interface of thermostat applied and free regions, while the resistance of the isothermal region is naturally zero. For Berendsen and Nose-Hoover we used the same damping factor employed in the Langevin thermostat. As stated earlier, artificial thermal resistance is consistently observed between the thermostat applied and thermostat free Silver layers for these thermostat techniques. Different thermostating approaches result in different reservoir temperatures, heat flux values and temperature jumps. Specifically, measured hot reservoir temperatures are 139.8, 138.65 and 138.9 K (140 K is imposed) and heat flux values are 5.91×10^8, 6.18×10^8 and 6.20×10^8 W/m^2, while the temperature jumps at the hot reservoir are 2.4, 0.35 and 0.3 K for the Langevin, Berendsen and Nose-Hoover thermostats, respectively. As a result, the calculated artificial thermal resistance of Langevin, Berendsen and Nose-Hoover cases using Eq. (8) are equal to 4×10^{-9}, 0.56×10^{-9} and 0.48×10^{-9} $K\,m^2/W$, respectively. Depending on the approach, thermostat maintaining the reservoir temperature close to the assigned value strongly alters the particle motions and greatly affects the intramolecular interactions between the thermostat applied and thermostat free solid layers. An important aspect of this observation is the relative importance of these artificial thermal resistance values to the physical Kapitza resistance values. For Langevin thermostat, the artificial resistance is the same order of magnitude as the Kapitza resistance at the liquid-solid interface. On the other hand, Berendsen and Nose-Hoover thermostats result in artificial resistance values that are about 10% of the Kapitza resistance. The lack of match between the target and resulting temperatures for the Berendsen and Nose Hoover thermostats was addressed by adding a controller to the measured and target temperature, as previously shown in [5].

3.3. Constant heat flux

In an NVT ensemble, the main aim of the thermostat mechanism is keeping the temperature constant. Thermostat adding energy to the molecules at an incident when their instantaneous temperature is lower than the desired value, may remove energy from the same group of molecules if their temperature is higher at any following time step. This behavior corrupts the vibrational nature of the material and affects phonon transfer, resulting in a temperature jump between the thermostat applied and free regions. Instead of assigning a constant surface temperature using a thermostat, one can maintain heat flux in the system by simply injecting and removing energy from the left and right heat baths, respectively. Different than using a thermostat, non-translational kinetic energy is added to the molecules of hot reservoir (and removed from the molecules of the cold reservoir) at every time step continuously, regardless of their instantaneous temperatures. In such case, NVE ensemble is obtained where the *heat flow is constant* and the surface temperature fluctuates. This approach is identical to the solution of heat conduction problem by assigning heat flux (Neumann boundary condition) on both boundaries, which makes the continuum solution of heat conduction equation ill-posed, due to the undetermined integration constant that fixes the temperature value. MD simulation of such a case has similar difficulties. Since the energy is added and removed at a constant rate, the surface temperature is continuously adjusted, and hence, actual temperature of the surface cannot be assigned a priory. For such cases, the initial temperature of the system plays a key role to obtain the desired temperature. For example, in order to create a case with 140–90 K surface temperatures, simulation should initially be brought to thermal equilibrium at 115 K, which is the average temperature. Then, energy is added and removed from the left and right walls, respectively, while the heat flux value is adjusted to obtain the desired temperature difference of $\Delta T \approx 50$ K between the two reservoirs. The temperature profile in the system, obtained by adding and removing energy from outermost three layers of the left and right Silver slabs (Case 5) is shown in Fig. 8. Unlike the cases that utilized thermostat, adding energy does not create unphysical temperature jumps inside the solid domains. Similar to the previous cases, we calculated the L_k values at the liquid/solid interface, which are 5.9 Å and 3.0 Å on the 139.8 K and 90.9 K surfaces, respectively (Table 2). Consistent with our earlier observations, the Kapitza lengths obtained by adding heat are similar with Case 2, which utilized thermostat on outermost three layers of the walls. Since adding and removing energy from the solid domains eliminate the artificial thermal resistance observed in thermostat applied systems, this method seems to be the most proper way to investigate the interface thermal resistance using non-equilibrium molecular dynamics simulations.

Since adding and extracting energy do not create unphysical temperature jumps in solid domains, it may be computationally more efficient to reduce the number of wall layers in simulations. In Case 6, we created silver walls using only four layers. The outermost silver layer is fixed to create a constant simulation volume, and energy is added/extracted from the remaining three wall layers. Specifically choosing three wall layers is due to the current cut-off distance of pair wise interactions and the spacing between each Silver layer. Fig. 9 illustrates the temperature profiles in Cases 6 and 5. Surprisingly the temperature profiles for both cases are parallel to each other. This shows the inability of MD to exactly fix the desired temperature in the system by assigning an initial temperature to the domain. Calculated L_k values for both cases are similar (Table 2) to each other, validating that there is no need to model larger simulation domains. Thermal resistance for each

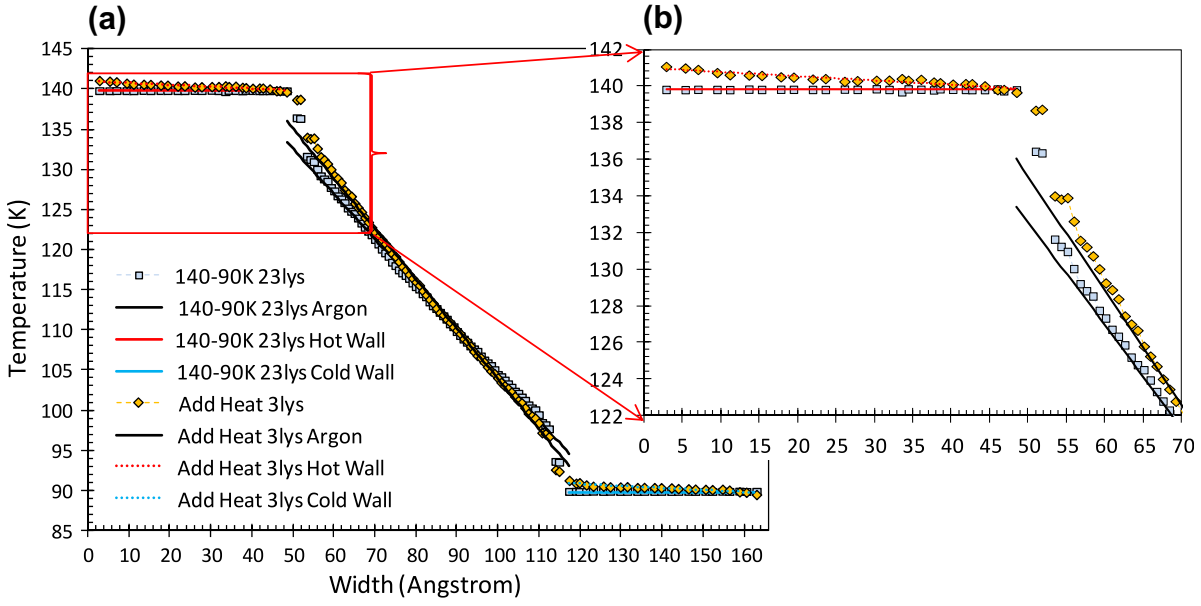

Fig. 8. Temperature profile when energy is added and removed from three outermost layers of Silver walls (Case 5). Result of Case 1 is plotted for comparison (a). Zoomed view of the hot surface shows elimination of the artificial thermal resistance in Case 5 (b).

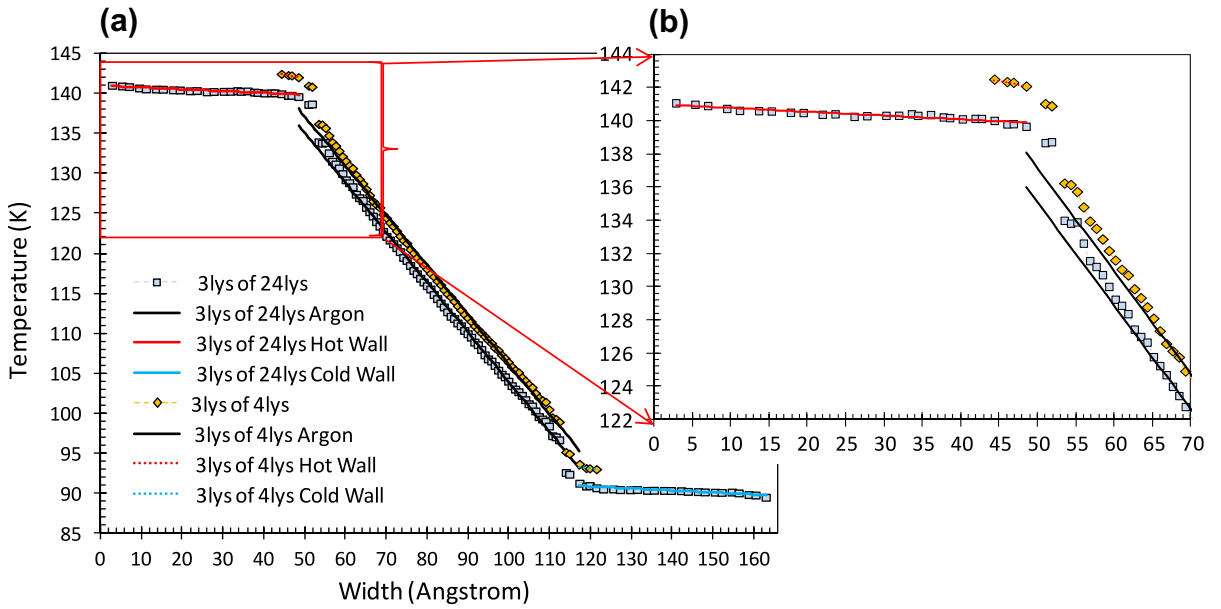

Fig. 9. Temperature profiles when energy is added and removed from 3 outermost layers of walls consisting of 24 (Case 5) and 4 (Case 6) Silver layers (a). Zoomed view of the hot surfaces (b).

component of Cases 5 and 6 are also shown in Table 4. Limited number of Silver layers in Case 6 seems to alter the thermal resistance of the solid domain. Difference in the resistance of Argon regions is due to the different average liquid temperatures, which is lower in Case 5 than Case 6. Overall, the Kapitza resistance values for both cases are similar to each other.

4. Conclusions

Using three distinct boundary treatment methods we investigated heat conduction in liquid Argon filled Silver nanochannels with the objective of characterization of the Kapitza resistance using non-equilibrium Molecular Dynamics method. The first and most common approach utilizes constant temperature surfaces imposed via a thermostat (Case 1). However, the Kapitza resistance calculated with this method results in artificially large values, compared with Case 2, which thermostats the outermost three wall layers. In fact, Case 2 exhibits artificial resistance at the edge of the thermostat applied region as an unphysical temperature jump in the homogenous Silver domain. Detailed thermal resistance analysis of both cases clearly show that the isothermal wall approach suffers from the artificial thermal resistance on the liquid/solid interface, where MD predicted resistance value is a superposition of the physical Kapitza resistance and the artificial resistance due to the thermostat effects. The alternative approach of adding and extracting energy at three outermost layers of Silver walls (Case 5) eliminates the artificial thermal resistance, and results in Kapitza resistance values consistent with Case 2. However, this approach has its own limitations, such as the inability to assign wall temperature, which is similar to the undetermined temperature based on integration of heat conduction equation using Neumann boundary conditions. Unlike the continuum based approach, MD converges to a temperature distribution determined by the initial temperature of the system. Utilization of only four Silver layers (Case 6) by adding and extracting energy from three wall layers resulted in similar Kapitza resistance values, compared with the predictions of Case 5.

Results clearly show that the Kapitza resistance and Kapitza length should be predicted either by using a large solid domain by applying thermostat to several wall layers away from the liquid/solid interface, or by adding and extracting energy from the surfaces. The latter approach can utilize smaller number of wall layers and minimizes the computational burden of simulating large number of wall molecules. It is also shown that the artificial thermal resistance varies between 3.8×10^{-9} and 4.2×10^{-9} K m^2/W using a Langevin thermostat in 140–90 K range. The Kapitza resistance at liquid Argon Silver interface varies from 5.4×10^{-9} and 2.2×10^{-9} in the same temperature range.

Acknowledgement

This work was supported by the National Science Foundation under Grant No: CBET 0931988.

References

[1] G.E. Karniadakis, A. Beskok, N. Aluru, Micro Flows and Nano Flows: Fundamentals and Simulation, Springer-Verlag, New York, 2005.

[2] D.G. Cahill, W.K. Ford, K.E. Goodson, G.D. Mahan, A. Majumdar, H.J. Maris, R. Merlin, S.R. Phillpot, Nanoscale thermal transport, J. Appl. Phys. 93 (2003) 793.
[3] S. Maruyama, Molecular dynamics methods in microscale heat transfer, heat transfer and fluid flow in microchannel, Gian Piero Celata (2004) 161–205.
[4] M.P. Allen, D.J. Tildesley, Computer Simulation of Liquids, Clarendon, Oxford, 1987.
[5] K. Jolley, S.P.A. Gill, Modeling transient heat conduction in solids at multiple length and time scales: A coupled non-equilibrium molecular dynamics/continuum approach, J. Comput. Phys. 228 (2009) 7412–7425.
[6] P.K. Schelling, S.R. Phillpot, P. Keblinski, Comparison of atomic-level simulation methods for computing thermal conductivity, Phys. Rev. B 65 (2002) 144306.
[7] Z.X. Huang, Z.A. Tang, Evaluation of momentum conservation influence in non-equilibrium molecular dynamics methods to compute thermal conductivity, Physica B 373 (2006) 291–296.
[8] A. Maitia, G.D. Mahana, S.T. Pantelidesa, Dynamical simulations of nonequilibrium processes: Heat flow and the Kapitza resistance across grain boundaries, Solid State Commun. 102 (1997) 517–521.
[9] Q. Tang, A molecular dynamics simulation: the effect of finite size on the thermal conductivity in a single crystal silicon, Mol. Phys. 102 (2004) 1959–1964.
[10] P. Jund, R. Jullien, Molecular-dynamics calculation of the thermal conductivity of vitreous silica, Phys. Rev. B 59 (1999) 13707.
[11] H. Zhong, J.R. Lukes, Interfacial thermal resistance between carbon nanotubes: Molecular dynamics simulations and analytical thermal modeling, Phys. Rev. B 74 (2006) 125403.
[12] C. Schröder, V. Vikhrenko, D. Schwarzer, Molecular dynamics simulation of heat conduction through a molecular chain, J. Phys. Chem. A 113 (2009) 14039–14051.
[13] Y.W. Yang, X.J. Liu, J.P. Yang, Nonequilibrium molecular dynamics simulation for size effects on thermal conductivity of Si nanostructures, Mol. Simul. 34 (2008) 51–55.
[14] J. Chen, G. Zhang, B. Li, Molecular dynamics simulations of heat conduction in nanostructures: effect of heat bath, J. Phys. Soc. Jpn. 79 (2010) 074604.
[15] G.L. Pollack, Kapitza resistance, Rev. Mod. Phys. 41 (1969) 48–81.
[16] B.H. Kim, A. Beskok, T. Cagin, Thermal interactions in nanoscale fluid flow: molecular dynamics simulations with solid-liquid interfaces, Microfluid. Nanofluid. 5 (2008) 551–559.
[17] B.H. Kim, A. Beskok, T. Cagin, Molecular dynamics simulations of thermal resistance at the liquid-solid interface, J. Chem. Phys. 129 (2008) 174701.
[18] Ganesh. Balasubramanian, Soumik. Banerjee, Ishwar.K. Puri, Unsteady nanoscale thermal transport across a solid–fluid interface, J. Appl. Phys. 104 (2008) 064306.
[19] C. Liu, H.B. Fan, K. Zhang, M.M.F. Yuen, Z. Li, Flow dependence of interfacial thermal resistance in nanochannels, J. Chem. Phys. 132 (2010) 094703.
[20] S.J. Plimpton, Fast Parallel Algorithms for Short–Range Molecular Dynamics, J. Comput. Phys. 117 (1995) 1-19. see http://lammps.sandia.gov for more information.
[21] P.M. Agrawal, B.M. Rice, D.L. Thompson, Predicting trends in rate parameters for self-diffusion on FCC metal surfaces, Surf. Sci. 515 (2002) 21–35.
[22] S.M. Foiles, M.I. Baskes, M.S. Daw, Embedded-atom-method functions for the fcc metals Cu, Ag, Au, Ni, Pd, Pt, and their alloys, Phys. Rev. B 33 (1986) 7983–7991.
[23] X.W. Zhou, R.A. Johnson, H.N.G. Wadley, Misfit-energy-increasing dislocations in vapor-deposited CoFe/NiFe multilayers, Phys. Rev. B 69 (2004) 144113.
[24] S. Qu, V. Shastry, W.A. Curtin, R.E. Miller, A finite temperature dynamic coupled atomistic/discrete dislocation method, Modell. Simul. Mater. Sci. 13 (2005) 1101.
[25] P.A. Tipler, R. Llewellyn, Modern Physics, W.H. Freeman, fifth ed., New York, 2007.
[26] J.H. Irving, J.G. Kirkwood, The statistical mechanical theory of transport processes. IV. The equations of hydrodynamics, J. Chem. Phys. 18 (1950) 817–829.
[27] B.D. Todd, P.J. Daivis, D.J. Evans, Heat flux vector in highly inhomogeneous nonequilibrium fluids, Phys. Rev. E 51 (1995) 4362–4368.
[28] M. Barisik, A. Beskok, Equilibrium molecular dynamics studies on nanoscale confined fluids, Microfludics Nanofludics (2011), http://dx.doi.org/10.1007/s10404-011-0794-5.
[29] A.J.H. McGaughey, M. Kaviany, Thermal conductivity decomposition and analysis using molecular dynamics simulations. Part I. Lennard-Jones argon, Int. J. Heat Mass Transf. 47 (2004) 1783–1798.
[30] H.M. Roder, C.A. Nieto de Castro, U.V. Mardolcar, The thermal-conductivity of liquid argon for temperatures between 110-K and 140-K with pressures to 70 MPA, Int. J. Thermophys. 8 (1987) 521–540.
[31] M.S. Green, Markoff random processes and the statistical mechanics of time-dependent phenomena. II. Irreversible processes in fluids, J. Chem. Phys. 22 (1954) 398–413.
[32] R. Kubo, Statistical-mechanical theory of irreversible processes. I. General theory and simple applications to magnetic and conduction problems, J. Phys. Soc. Jpn. 12 (1957) 570–586.
[33] H.J.C. Berendsen, J.P.M. Postma, W.F. van Gunsteren, A. DiNola, J.R. Haak, Molecular-dynamics with coupling to an external bath, J. Chem. Phys. 81 (8) (1984) 3684–3690.
[34] D.J. Evans, W.G. Hoover, Flows far from equilibrium via molecular-dynamics, Annu. Rev. Fluid Mech. 18 (1986) 243–264.